

Article

# Pitting Corrosion of Steel Induced by Al<sub>2</sub>O<sub>3</sub> Inclusions

**Qing Liu** <sup>1,2</sup>, **Shufeng Yang** <sup>1,2,\*</sup>, **Mengjing Zhao** <sup>1,2</sup>, **Libin Zhu** <sup>1,2</sup> and **Jingshe Li** <sup>1,2</sup>

<sup>1</sup> School of Metallurgical and Ecological Engineering, University of Science and Technology Beijing, Beijing 100083, China; m18347267087\_1@163.com (Q.L.); ustbzhaomengjing@163.com (M.Z.); zhulibin1234567890@163.com (L.Z.); lijingshe@ustb.edu.cn (J.L.)

<sup>2</sup> Beijing Key Laboratory of Special Melting and Preparation of High-End Metal Materials, Beijing 100083, China

\* Correspondence: yangshufeng@ustb.edu.cn; Tel.: +86-185-1169-5668

Received: 13 July 2017; Accepted: 26 August 2017; Published: 5 September 2017

**Abstract:** To study the effect of Al<sub>2</sub>O<sub>3</sub> inclusions on pitting corrosion in steel, our researchers utilized industrial pure iron as the raw material with the addition of a proper amount of pure aluminum powder to form Al<sub>2</sub>O<sub>3</sub> inclusions. Corrosion experiments were performed by exposing the samples to a 6% FeCl<sub>3</sub> solution at room temperature (25 °C) for different lengths of time. Microscopic corrosion morphology was observed by scanning electron microscope (SEM), and the size change of the inclusions was quantitatively analyzed with Image Pro Plus. The experimental results showed that pitting corrosion arose preferentially around the Al<sub>2</sub>O<sub>3</sub> inclusions, and that pitting corrosion initiated at the junction of the Al<sub>2</sub>O<sub>3</sub> inclusions. The steel matrix dissolved and micro-cracks occurred as the Al<sub>2</sub>O<sub>3</sub> inclusions that were buried shallowly below the surface of the steel matrix promoted corrosion of the steel matrix. As corrosion progressed, the shallowly buried Al<sub>2</sub>O<sub>3</sub> inclusions began to appear on the surface, and the small, shallow inclusions fell off and formed micro pits. Furthermore, the clustered distribution of alumina inclusions had a greater effect on pitting initiation than the alumina inclusions distributed alone.

**Keywords:** Al<sub>2</sub>O<sub>3</sub> inclusions; pitting corrosion; initiation; steel

## 1. Introduction

Currently, corrosion damage is the most serious problem for steel materials, and has a close relationship with the national economy and defense construction [1]. Corrosion triggers can be broadly divided into two types: internal metallurgical factors and external environmental factors. Internal metallurgical factors include the shape, distribution, size of inclusions, chemical composition, steel microstructure, and so on. External environmental factors include temperature, pH, and corrosion environment [2]. Pitting corrosion is a type of localized corrosion [3,4], and is often an initial state for other forms of corrosion [5]. For example, it can act as an initiation site for stress corrosion cracks [6]. If pitting corrosion is uncontrolled, it often results in early failure of the equipment, leading to direct loss, indirect loss, and incalculable economic consequences [7]. Thus, pitting corrosion plays a key role in the whole corrosion process, and the study of the influencing factors triggering pitting corrosion is evidently important.

The pitting corrosion process is divided into two stages: pit initiation and pit propagation [8]. Many researchers have studied the pitting processes, with most of them acknowledging that non-metallic inclusions induced pitting corrosion [9–12]. Schmuki et al. [13] observed the inclusions in high sulfur stainless steel and found that the surroundings of the inclusions were preferentially dissolved and pitting corrosion occurred at the inclusions or their surroundings. Chiba et al. observed that the metastable and stable pits were initiated at the MnS/steel boundaries [14]. Zheng et al. [15]

observed two types of inclusions in 316L stainless steel made of composite oxide inclusions of Ca, Mg, and Al, and alumina inclusions, respectively. Furthermore, they indicated that these two types of inclusions could trigger pitting corrosion in  $\text{Cl}^-$  solution. They also established the pitting inducing mechanism where Mg, Al, and Ca composite oxide inclusions were corroded in a sulfur environment containing chloride ions. Compared with  $\text{Al}_2\text{O}_3$  inclusions, pitting corrosion occurred more easily at the junction of the steel matrix and Mg, Al, Ca composite oxide inclusion. Muto et al. [16] conducted pitting corrosion micro-electrochemical experiments of sulfide and oxide inclusions in 304 stainless steel. They observed that MnS/CrS inclusions were more likely to be sites of pitting initiation rather than the  $\text{MnO}/\text{CrO}$  inclusions. In addition, pitting corrosion occurred at the boundary of the oxide inclusions and steel matrix in the FESEM (Field Emission Scanning Electron Microscope) images, which was consistent with the observation of sulfide inclusions.

Practically, aluminum killed steel accounts for a large proportion of industrial steel, and the deoxidation products mainly contain Al inclusions [17,18].  $\text{Al}_2\text{O}_3$  is the most typical non-metallic inclusion, and has been widely studied in papers [19,20]. The distribution of the  $\text{Al}_2\text{O}_3$  inclusions and surface defects caused by  $\text{Al}_2\text{O}_3$  inclusions has an important effect on the corrosion of steel materials, but there is less research on the effects of  $\text{Al}_2\text{O}_3$  on pitting corrosion of steel materials. We studied the influence of  $\text{Al}_2\text{O}_3$  inclusions with different distribution forms on pitting corrosion, which will be of great significance to further avoid corrosion in the metallurgical production process.

## 2. Experimental Procedures

### 2.1. Preparation and Processing of Experimental Materials

The experimental material used was industrial pure iron, and its chemical composition is shown in Table 1.

**Table 1.** Chemical compositions (mass %).

C	Si	Mn	P	S	Al	Ni	Cr	Cu	Ti
0.003	0.03	0.05	0.010	0.006	0.03	0.03	0.02	0.03	0.02

Multiple samples with a size of  $10 \times 10 \times 15 \text{ mm}^3$  were cut using a wire cutting machine for ingot symmetry (DK7732 wire cutting machine, Kingred, Suzhou, China). The  $10 \times 10$  side of the sample was used as the working surface of the test sample. The working surface was sanded with SiC sandpapers and then polished. Finally, distilled water and anhydrous ethanol were used to wash the working surface. The inclusions were observed by scanning electron microscopy (SEM, Phenom proX scanning electron microscopy, Eindhoven, The Netherlands).

### 2.2. Experimental Schemes

Industrial pure iron was melted in a corundum crucible. The experiments were performed using a tubular resistance furnace with  $\text{MoSi}_2$  heating bars under an Ar atmosphere (SK168YL tubular resistance furnace, Beijing, China). When the steel temperature reached 1873 K (1600 °C), it was kept at this temperature for 30 min before an appropriate amount of pure aluminum powders were added to the molten steel to generate  $\text{Al}_2\text{O}_3$  inclusions. Once the  $\text{Al}_2\text{O}_3$  inclusions in the samples were generated, their compositions were obtained and morphology was observed using scanning electron microscope and energy dispersive spectroscopy (SEM-EDS).

The samples were immersed for different immersion time in 6%  $\text{FeCl}_3$  solution (with reference to national standard GB/T 17897-2016) at room temperature (25 °C). When they reached the set time, the samples were quickly removed from the solution, rinsed with distilled water and anhydrous ethanol, and then blow-dried. The samples were observed and analyzed by SEM, and then immersed back in the solution to continue the exposure. So, the microscopic corrosion morphology of the samples

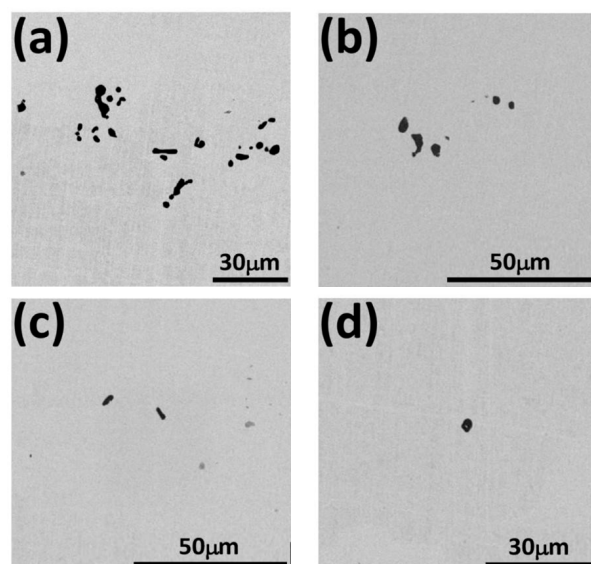
at different immersion time were observed. Changes in inclusion size during the process of corrosion were quantitatively analyzed using Image Pro Plus software (Version 6.0, Media Cybernetics, Inc., Rockville, MD, USA). In the meantime, it could also obtain the change of  $\text{Al}_2\text{O}_3$  inclusions in the same location during the corrosion process.

### 3. Results and Discussion

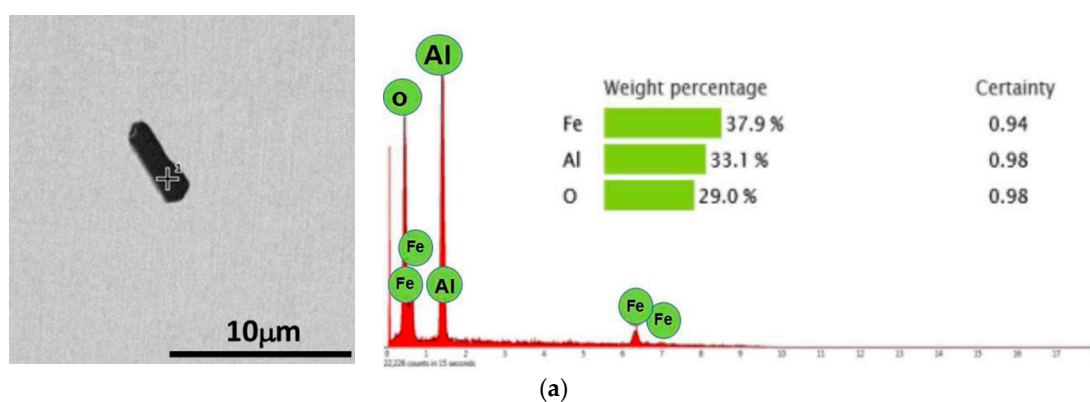
#### 3.1. Observation and Control of $\text{Al}_2\text{O}_3$ Inclusions

Figure 1 represents the typical  $\text{Al}_2\text{O}_3$  inclusions found in the samples. According to the experimental results,  $\text{Al}_2\text{O}_3$  inclusions were classified into four types: (1) a large number of  $\text{Al}_2\text{O}_3$  inclusions gathered together to form a cluster distribution, as shown in Figure 1a; (2) a small amount of  $\text{Al}_2\text{O}_3$  gathered together (generally between 3–6), as shown in Figure 1b; (3) Figure 1c indicates that  $\text{Al}_2\text{O}_3$  inclusions were long strip-shaped and with a lone distribution; and (4) Figure 1d shows that  $\text{Al}_2\text{O}_3$  inclusions were mainly irregular in shape.

Figure 2 shows the composition analysis of typical  $\text{Al}_2\text{O}_3$  inclusions. Through the EDS results, it was concluded that the inclusions in the samples were  $\text{Al}_2\text{O}_3$  inclusions.



**Figure 1.** SEM (Scanning Electron Microscope) images of  $\text{Al}_2\text{O}_3$  inclusions from sample: (a) a large number of  $\text{Al}_2\text{O}_3$  inclusions gathered together to form a cluster distribution; (b) a small amount of  $\text{Al}_2\text{O}_3$  gathered together; (c)  $\text{Al}_2\text{O}_3$  inclusions were long strip-shaped and with a lone distribution; (d)  $\text{Al}_2\text{O}_3$  inclusions were mainly irregular in shape.



**Figure 2. Cont.**

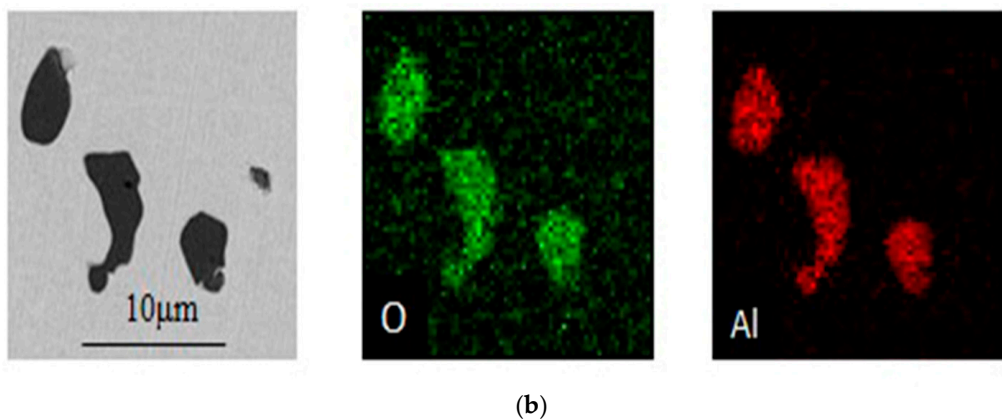
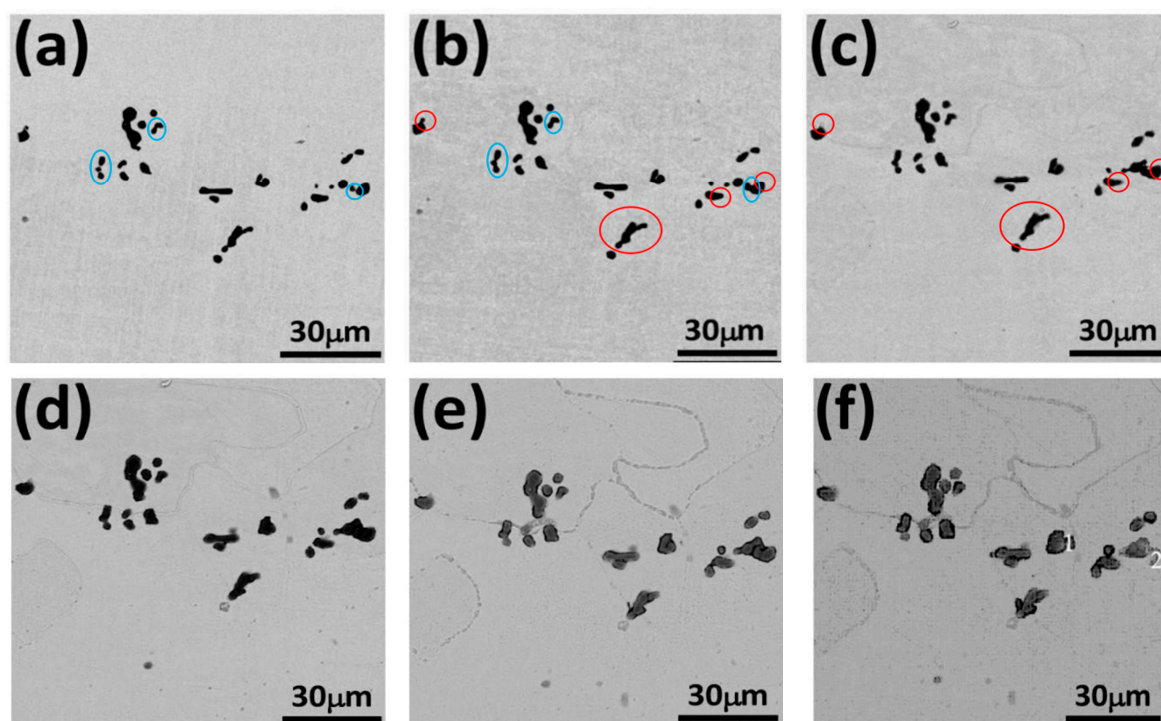


**Figure 2.** EDS (Energy Dispersive Spectroscopy) results of the typical Al<sub>2</sub>O<sub>3</sub> inclusion from sample. (a) Point scan analysis; and (b) elemental distribution in Al<sub>2</sub>O<sub>3</sub> inclusion.

### 3.2. Study on Corrosion Induced by Al<sub>2</sub>O<sub>3</sub> Inclusions

#### 3.2.1. Effect of Clustered Al<sub>2</sub>O<sub>3</sub> Inclusions on Corrosion

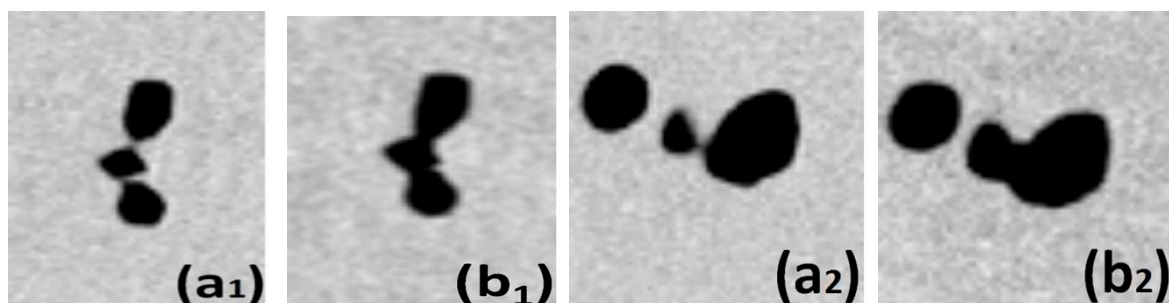
Samples were tested at different time of corrosion immersion with 6% FeCl<sub>3</sub> solution at room temperature (25 °C). The microscopic corrosion morphology of the same location under different immersion time was observed by scanning electron microscopy to study the effect of Al<sub>2</sub>O<sub>3</sub> inclusions on pitting corrosion. As the Al<sub>2</sub>O<sub>3</sub> inclusions had a high interfacial energy, the inclusions in the molten steel easily gathered to form a clustered distribution through collision and coalescence [21]. The SEM images of the Al<sub>2</sub>O<sub>3</sub> inclusions in a clustered distribution are shown in Figure 3. Image Pro Plus software was used for the quantitative analysis of inclusions categorized by size to obtain the changes in Al<sub>2</sub>O<sub>3</sub> inclusions at the same location during the process of corrosion.



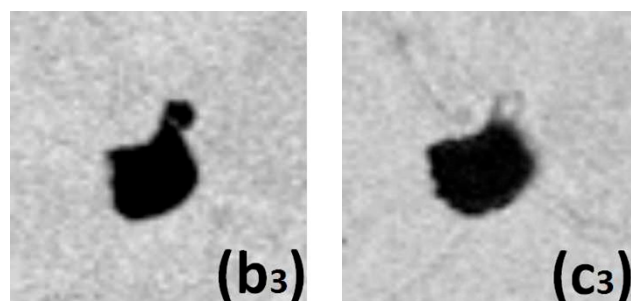
**Figure 3.** Morphology observation of clustered Al<sub>2</sub>O<sub>3</sub> inclusions: (a) 0 s; (b) 15 s; (c) 35 s; (d) 65 s; (e) 105 s; and (f) 155 s.

A comparison of Figure 3a,b shows that the  $\text{Al}_2\text{O}_3$  inclusions and steel matrix had almost no significant changes. Furthermore, it was found that the dissolution of single  $\text{Al}_2\text{O}_3$  with a relatively small spacing was transferred to other adjacent inclusions (blue circles) to form a little larger area of pitting corrosion. Figure 4 is the local enlarged image of Figure 3. It was found that there was a small spacing between the inclusions at 0 s, which disappeared after 15 s, and indicated that the  $\text{Al}_2\text{O}_3$  inclusions induced pitting corrosion where the matrix was dissolved. Instead, the samples only presented slight corrosion under corrosion immersion at 15 s.

Figure 3c shows the morphology for further corrosion. Since there were more light-colored corrosive products (blurred gray) around the inclusions (compared red circles in Figure 3b,c), it was obvious that pitting corrosion occurred at the junction of  $\text{Al}_2\text{O}_3$  inclusions and its adjacent steel matrix. Additionally, part of the  $\text{Al}_2\text{O}_3$  inclusions had fallen off, as shown in the far-left figure. The local enlarged drawing is shown in Figure 5.



**Figure 4.** Graphs are local enlarged diagrams (a<sub>1</sub>) 0 s; (b<sub>1</sub>) 15 s; (a<sub>2</sub>) 0 s; (b<sub>2</sub>) 15 s.



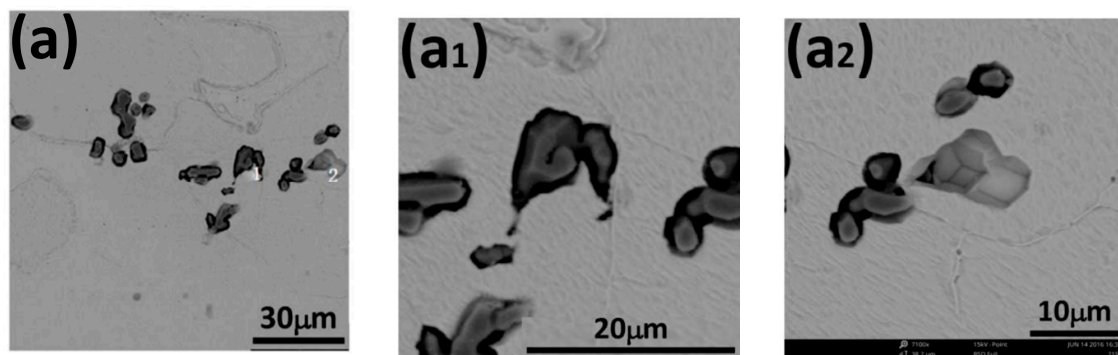
**Figure 5.** Graphs are local enlarged diagrams (b<sub>3</sub>) 15 s; and (c<sub>3</sub>) 35 s.

Figure 3e clearly shows the formation of micro gaps between the  $\text{Al}_2\text{O}_3$  inclusions and steel matrix. By using Image Pro Plus software to compare the size of  $\text{Al}_2\text{O}_3$  inclusions before and after corrosion, it was found that the average size of  $\text{Al}_2\text{O}_3$  inclusions increased, which indicated that the steel matrix adjacent to the inclusions dissolved and the  $\text{Al}_2\text{O}_3$  inclusions originally buried in the steel matrix were partially exposed. Thus, it was concluded that the formation of the micro gap was mainly caused by the dissolution of the steel matrix adjacent to the inclusions.

Figure 3f shows the  $\text{Al}_2\text{O}_3$  inclusions at Position 1 were significantly larger than that in previous pictures (the same location in Figure 3a–e) due to the dissolution of the steel matrix near the inclusions. Furthermore, the  $\text{Al}_2\text{O}_3$  inclusions at Position 2 partially disappeared and fell off to form micro pits. Additionally, some of the inclusions disappeared, indicating that pitting corrosion occurred along the junction between the  $\text{Al}_2\text{O}_3$  inclusions and steel matrix; and  $\text{Al}_2\text{O}_3$  inclusions buried shallowly in the steel matrix fell off and formed micro pits.

Figure 6 shows the corrosion morphology of the samples at 215 s. The area of  $\text{Al}_2\text{O}_3$  inclusions at Position 1 was further increased with respect to 155 s, and the local enlarged image is shown in Figure 6a<sub>1</sub>. By using Image Pro Plus software to measure the area of  $\text{Al}_2\text{O}_3$  inclusions, it was found

that the area of  $\text{Al}_2\text{O}_3$  inclusions increased from  $44.83 \mu\text{m}^2$  to  $65.81 \mu\text{m}^2$  and the size of the micro gap between the inclusions and the steel matrix was larger. These phenomena resulted from the further dissolution of the surrounding steel matrix, which was due to the formation of an occlusion zone; other locations of the  $\text{Al}_2\text{O}_3$  inclusions also showed similar phenomena. The area of the micro pits at Position 2 increased from  $72.19 \mu\text{m}^2$  at 155 s to  $81.88 \mu\text{m}^2$  at 215 s. Furthermore, it was noteworthy that new  $\text{Al}_2\text{O}_3$  inclusions appeared on the left side of the micro etch pits, and the local enlarged drawing is shown in Figure 6a<sub>2</sub>. In contrast, it was found that the increased areas of micro pits were mainly concentrated on the side of newly emerging  $\text{Al}_2\text{O}_3$  inclusions. This indicated that the presence of  $\text{Al}_2\text{O}_3$  inclusions had a positive effect on the increment of micro pits, and the inclusions fell off to form micro pits, which reduced the damage to the steel matrix.



**Figure 6.** The corroded morphology of clustered  $\text{Al}_2\text{O}_3$  at (a) 215 s; (a<sub>1</sub>) a local enlarged diagram of Position 1; and (a<sub>2</sub>) a local enlarged diagram of Position 2.

### 3.2.2. Effect of Lone Distributed $\text{Al}_2\text{O}_3$ Inclusions on Corrosion

In SEM morphology of lone distributed  $\text{Al}_2\text{O}_3$  inclusions is presented in Figure 7. Figure 7a–c reveal the corrosion morphology of the specimen under short immersion time. It was observed that the pitting-induced location was at the junction of the  $\text{Al}_2\text{O}_3$  inclusion and its adjacent steel matrix. By comparing the changes of  $\text{Al}_2\text{O}_3$  inclusion at different time, it was found that the  $\text{Al}_2\text{O}_3$  inclusions did not dissolve. Thus, the formation of the micro-gaps was due to the dissolution of the adjacent steel matrix, which was the same as the pitting-induced regularity of clustered  $\text{Al}_2\text{O}_3$  inclusions.

Figure 7 shows further corrosion morphology. It was observed that the edge of  $\text{Al}_2\text{O}_3$  inclusions appeared to be corrosion products from the steel matrix. The corrosion products were lighter in color compared to the  $\text{Al}_2\text{O}_3$  inclusions. As the  $\text{Al}_2\text{O}_3$  inclusions were covered by the corrosion products of the steel matrix, the dissolution of the adjacent steel matrix was obviously subsided. This indicated that with the dissolution of the steel matrix, corrosion products increased, which has a certain degree of inhibition on the development of corrosion.

Figure 7e,f shows the corrosion morphology at longer immersion time, where the edge of  $\text{Al}_2\text{O}_3$  inclusions obviously dissolved, thus it was concluded that the corrosion products of the steel matrix were unstable. From Figure 7b, we could find that a micro-gap appeared between the steel matrix and inclusion (the picture showed the color of micro-gap is darker than that of inclusions). From Figure 7c–f, the micro-gap is growing larger, based on the position of Figure 7b. It was also noted that the dissolved edge of  $\text{Al}_2\text{O}_3$  inclusions were concentrated on the larger gaps between the steel matrix and inclusions (compared with Figure 7b), the reason being that the concentration of dissolved iron ions (which were produced in the larger cracks of the steel matrix) was higher. The hydrolysis degree of the iron ions was large, thereby resulting in low pH, where the edges of the  $\text{Al}_2\text{O}_3$  inclusions dissolved.

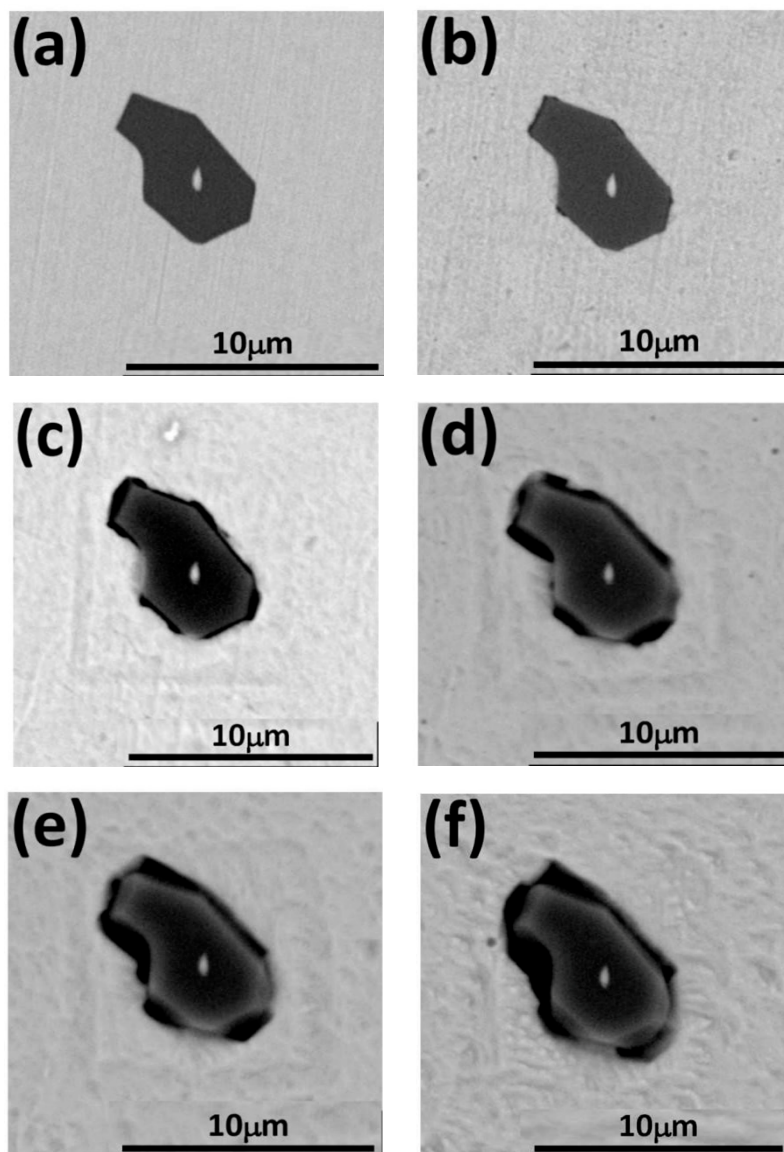


**Figure 7.** Morphology observation of singly distributed  $\text{Al}_2\text{O}_3$  inclusions. (a) 0 s; (b) 15 s; (c) 35 s; (d) 65 s; (e) 105 s; and (f) 155 s.

Figure 8 compares the map analysis results of the two immersion time of 0 and 65 s. It was found that the distribution of elemental Al in the  $\text{Al}_2\text{O}_3$  inclusions was consistent with the shape of the inclusions at 0 s and the edge of inclusions also had an obvious contour. While the distribution of elemental Al at 65 s had no obvious contour at the edge, elemental Al was also detected in the micro gap, which indicated that the  $\text{Al}_2\text{O}_3$  inclusions dissolved. Compared to 0 s, the content of the O element at the edge became higher at 65 s due to the reaction of oxygen absorption occurring during the corrosion process and produced iron oxides and hydroxides that covered the edges of the inclusions. The results of the elemental composition analysis of the inclusions were in good agreement with the corrosion morphology of Figure 7.

The above phenomena were also observed in the shorter strip-like  $\text{Al}_2\text{O}_3$  inclusions and a small amount of clustered  $\text{Al}_2\text{O}_3$  inclusions, as shown in Figure 9. Figure 10 shows the following phenomena observed in the corrosion morphology. The  $\text{Al}_2\text{O}_3$  inclusions were still in the steel matrix at 35 s. Furthermore, the inclusions were not visible on the SEM image at 65 s, leaving only the pits. Since the  $\text{Al}_2\text{O}_3$  inclusions were not easily dissolved, the formation of the etch pits was caused by the shedding

of the inclusions. This also showed that corrosion occurred along the junction of the inclusions and steel matrix. The number of small, shallow  $\text{Al}_2\text{O}_3$  inclusions in the adjacent steel matrix was less, as the inclusions separated from the steel matrix and fell off when the adjacent steel matrix dissolved.

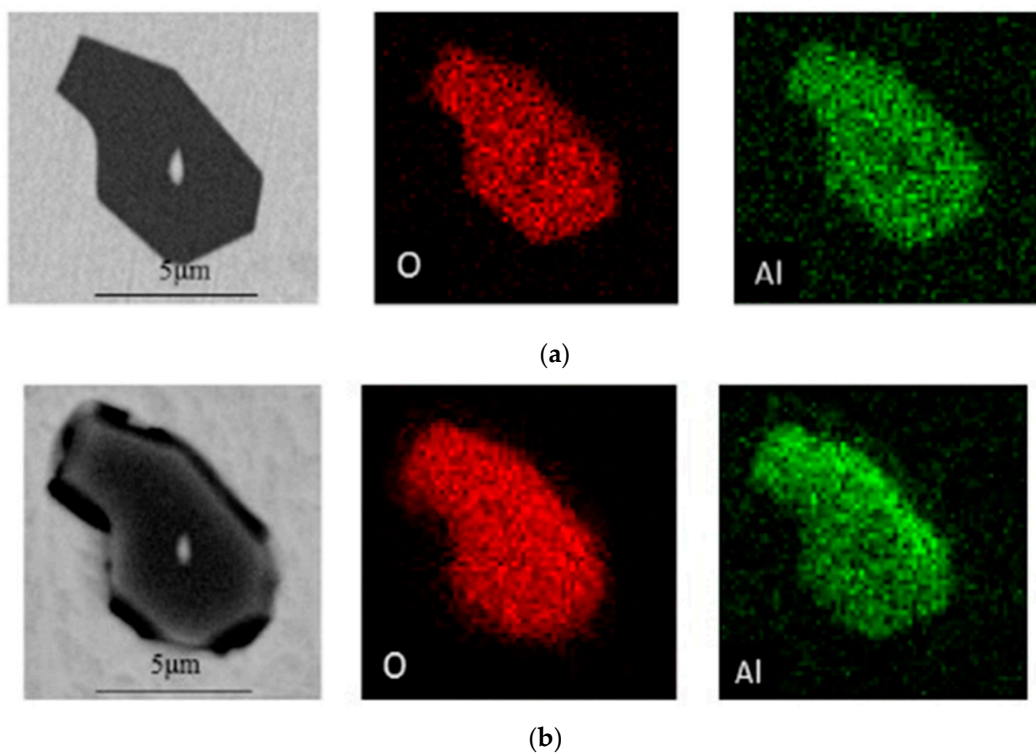


**Figure 8.** Analysis of  $\text{Al}_2\text{O}_3$  inclusions at different immersion time. (a) 0 s; and (b) 65 s.

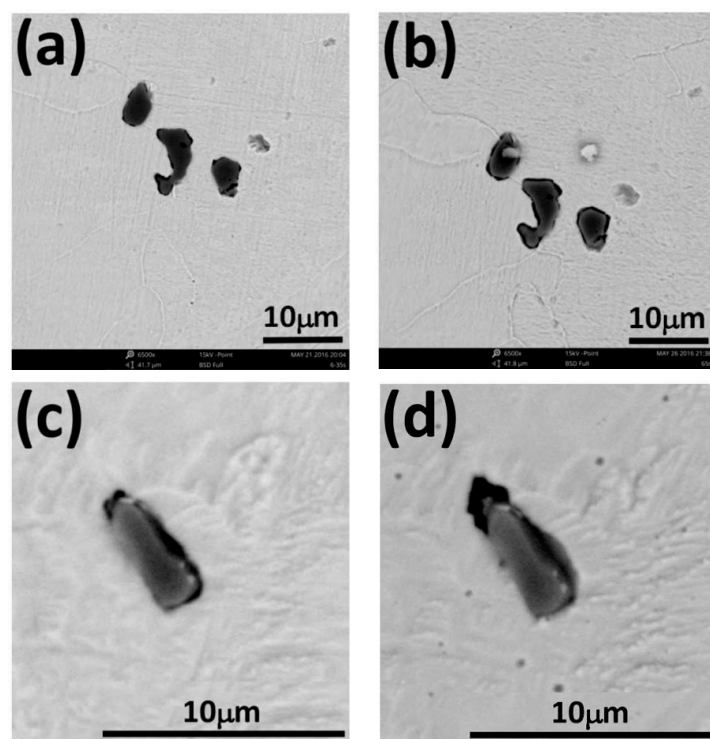


**Figure 9.** Other types of  $\text{Al}_2\text{O}_3$  inclusion corrosion morphology. (a) 35 s; (b) 65 s; (c) 105 s; (d) 155 s.

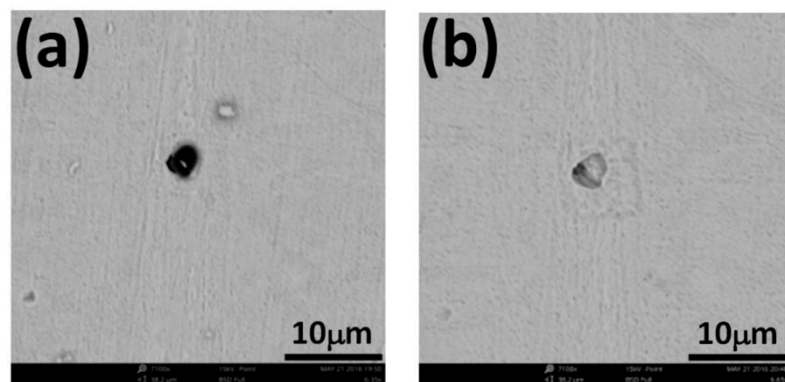


**Figure 10.**  $\text{Al}_2\text{O}_3$  inclusions fall off. (a) 35 s; and (b) 65 s.

During the process of corrosion immersion, a certain field of view of the specimen was observed, as shown in Figure 11. Figure 11a shows the morphology of corrosion at 35 s.  $\text{Al}_2\text{O}_3$  inclusions were not observed. When the samples were corroded for 65 s, inclusions occurred, as shown in Figure 11b (black dots).  $\text{Al}_2\text{O}_3$  inclusions appearing as inclusions buried on the surface of the steel matrix can promote corrosion in the steel matrix. With the dissolution of the steel matrix, the  $\text{Al}_2\text{O}_3$  inclusions buried in the steel matrix began to appear, and as the corrosion progressed, the size of the  $\text{Al}_2\text{O}_3$  inclusions became larger at 105 s, as shown in Figure 11c, because the inclusions near the steel matrix dissolved. Figure 11d shows that the size of the inclusions was further enlarged. This indicated that the inclusions buried shallowly in the surface of the steel matrix began to appear. As the corrosion progressed, the size of the inclusions became larger and once the inclusions appeared on the surface of the matrix, they caused a great deal of damage to the adjacent steel matrix. It was also proven that inclusions have an important effect on the corrosion of the steel matrix.

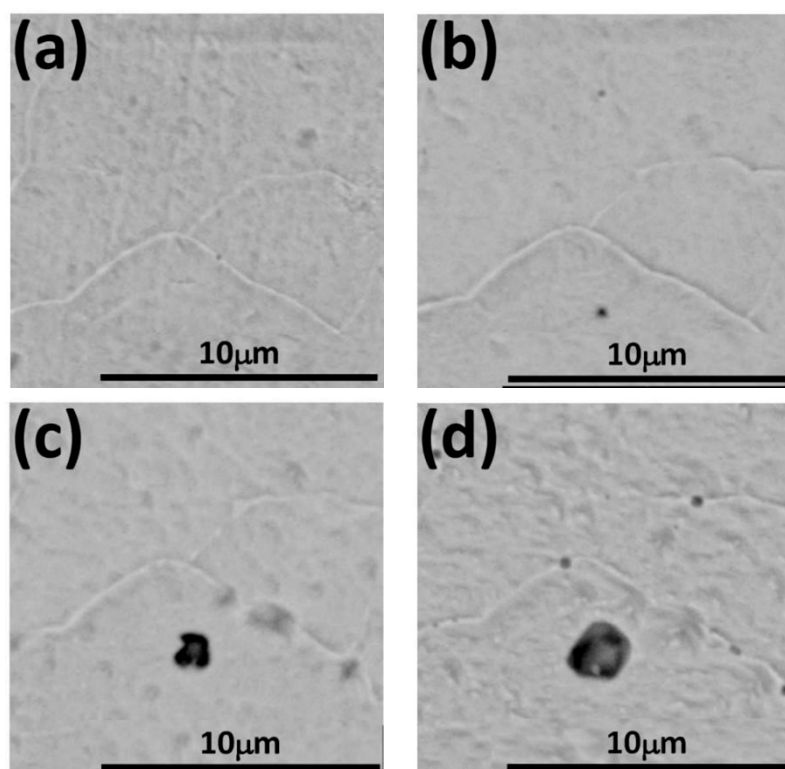


**Figure 11.** The surface morphology of the specimen changes: (a) 35 s; (b) 65 s; (c) 105 s; and (d) 155 s.

### 3.2.3. Analysis of Corrosion Induced Mechanism of $\text{Al}_2\text{O}_3$ Inclusions

The corrosion mechanisms are shown in Figure 12.  $\text{Al}_2\text{O}_3$  inclusions have a higher potential than the steel matrix and can form micro-corrosion batteries with the steel matrix. Due to a different structure or non-uniformity of components of the boundary between  $\text{Al}_2\text{O}_3$  inclusions and steel matrix [22,23], the steel matrix was unstable, the grain boundary energy was high, and the ionization tendency was great [24,25]. At the same time, the presence of inclusions broke the continuity of the passive film and the boundary was weakly protected by the passive film, as shown in Figure 12a–c. Thus, pitting corrosion was preferentially induced at the boundaries. The steel matrix adjacent to the inclusions dissolved, resulting in the production of micro gaps that formed a self-catalyzed activation-passivation corrosion battery based on the occlusion battery [26]. This caused the cracks to expand and corrosion pits to become deeper. The clustered  $\text{Al}_2\text{O}_3$  inclusions were more destructive to the steel matrix than the lone  $\text{Al}_2\text{O}_3$  inclusions. As the corrosion took place along the direction of the presence of inclusions, the clusters of  $\text{Al}_2\text{O}_3$  inclusions accelerated the corrosion process. Small and shallow  $\text{Al}_2\text{O}_3$  inclusions in the corrosion process easily fell from the steel matrix and formed the pits, thus weakening the harmful impacts on the steel matrix.

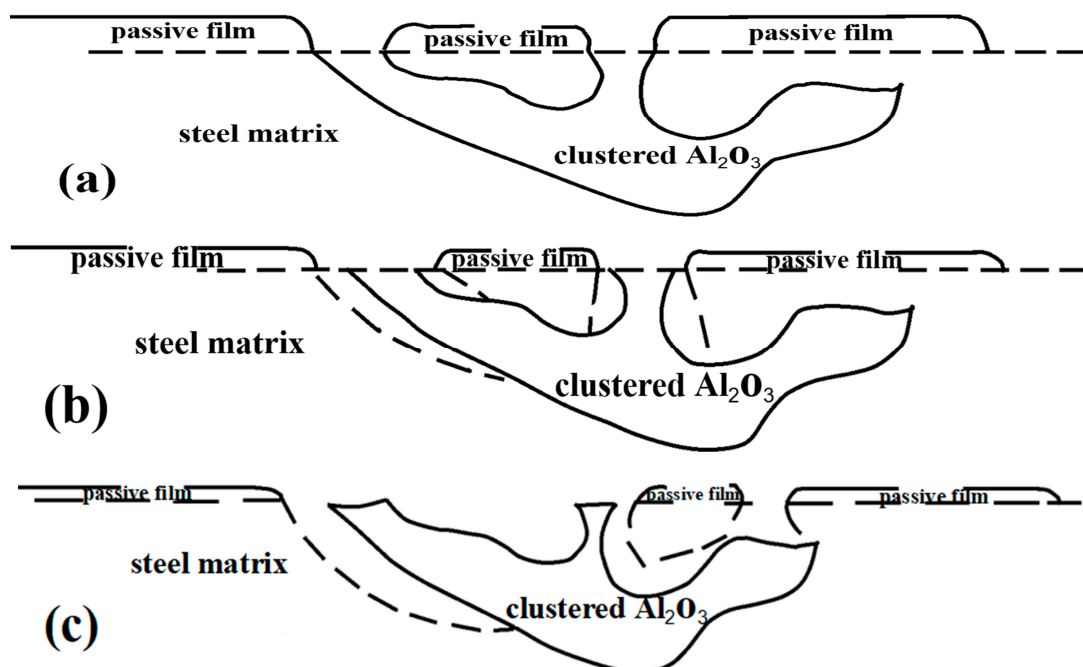


**Figure 12.** Corrosion mechanism diagram: (a) before corrosion; (b) during corrosion; (c) after corrosion.

## 4. Conclusions

The  $\text{Al}_2\text{O}_3$  inclusions were stable during a short period of corrosion immersion. During the process of corrosion, the inclusions did not dissolve. Therefore, pitting corrosion was induced at the boundary between the inclusions and the steel matrix, and the steel matrix dissolved to produce micro gaps. As the corrosion progressed, the size of the micro-cracks became larger, so the formation of the corrosive products could be clearly observed, and the edge of the  $\text{Al}_2\text{O}_3$  inclusions also dissolved.

The  $\text{Al}_2\text{O}_3$  inclusions not deeply buried on the surface of the steel matrix promoted corrosion in the steel matrix. With the dissolution of the steel matrix,  $\text{Al}_2\text{O}_3$  inclusions shallowly embedded in the steel matrix began to appear, and the size of inclusions increased slightly. Due to the dissolution of the steel matrix, small and shallow  $\text{Al}_2\text{O}_3$  inclusions fell off and formed micro pits.

Clustered  $\text{Al}_2\text{O}_3$  inclusions had a greater impact on pitting corrosion than lone  $\text{Al}_2\text{O}_3$  inclusions. As corrosion occurred around inclusions, the interaction of clustered  $\text{Al}_2\text{O}_3$  inclusions accelerated the dissolution of the adjacent steel matrix.

**Acknowledgments:** This research is supported by the National Science Foundation of China (Nos. 51474085 and 51474076) and the Joint Projects of USTB and NTUT (Grant No. TW201604).

**Author Contributions:** Qing Liu conceived and designed the experiments and interpreted the data; Qing Liu and Shufeng Yang wrote the paper; Mengjing Zhao analyzed the data and Libin Zhu performed the experiments; Jingshe Li collected the literature.

**Conflicts of Interest:** The authors declare no conflict of interest.

## References

1. Ke, W. Progress in public inquiry concerning corrosion in Chinese industrial and natural environments. *Corros. Prot.* **2004**, *25*, 1–8.
2. Frankel, G.S. Pitting corrosion of metals. *J. Electrochem. Soc.* **1998**, *145*, 2186. [[CrossRef](#)]
3. Song, Y.W.; Shan, D.Y.; Han, E.H. Pitting corrosion of a rare earth Mg alloy GW93. *J. Mater. Sci. Technol.* **2017**, *1*, 1–7. [[CrossRef](#)]
4. Williams, D.E.; Kilburn, M.R.; Cliff, J.; Waterhouse, G.I.N. Composition changes around sulfide inclusions in stainless steels, and implications for the initiation of pitting corrosion. *Corros. Sci.* **2010**, *52*, 3702–3716. [[CrossRef](#)]
5. Zhang, H.; Chen, X.Q.; Chang, W.S. Effect of metallurgy factors on susceptibility to pitting initiation in steels. *J. Chin. Soc. Corros. Prot.* **2009**, *29*, 127–131.
6. Caines, S.; Khan, F.; Shirokoff, J. Analysis of pitting corrosion on steel under insulation in marine environments. *J. Loss Prev. Proc.* **2013**, *26*, 1466–1483. [[CrossRef](#)]
7. Uhlig, H.H. The cost of corrosion to the United States. *Corrosion* **1950**, *6*, 29–33. [[CrossRef](#)]
8. Wang, J.M.; Chen, X.Q.; Li, G.M. Susceptibility of two types of low-alloy hull steels to pit initiation. *J. Univ. Sci. Technol. B* **2004**, *11*, 555–560.
9. Park, I.-J.; Lee, S.-M.; Kang, M.; Lee, S.; Lee, Y.-K. Pitting corrosion behavior in advanced high strength steels. *J. Alloys Compd.* **2015**, *619*, 205–210. [[CrossRef](#)]
10. Punckt, C.; Bölscher, M.; Rotermund, H.H.; Mikhailov, A.S.; Organ, L.; Budiansky, N.; Scully, J.R.; Hudson, J.L. Sudden onset of pitting corrosion on stainless steel as a critical phenomenon. *Science* **2004**, *305*, 1133–1136. [[CrossRef](#)] [[PubMed](#)]
11. Szkzarska-Smialowska, Z. The effect of inclusions on the susceptibility of steels to pitting, stress corrosion cracking and hydrogen embrittlement. *Mater. Corros.* **1981**, *32*, 478–485. [[CrossRef](#)]
12. Ha, H.Y.; Park, C.J.; Kwon, H.S. Effects of misch metal on the formation of non-metallic inclusions and the associated resistance to pitting corrosion in 25% Cr duplex stainless steels. *Scr. Mater.* **2006**, *55*, 991–994. [[CrossRef](#)]
13. Schmuki, P.; Hildebrand, H.; Friedrich, A.; Virtanen, S. The composition of the boundary region of MnS inclusions in stainless steel and its relevance in triggering pitting corrosion. *Corros. Sci.* **2005**, *47*, 1239–1250. [[CrossRef](#)]
14. Chiba, A.; Muto, I.; Sugawara, Y.; Hara, N. A microelectrochemical system for in situ high-resolution optical microscopy: morphological characteristics of pitting at MnS inclusion in stainless steel. *J. Electrochem. Soc.* **2013**, *26*, 1466–1483. [[CrossRef](#)]
15. Zheng, S.Q.; Li, C.Y.; Qi, Y.M.; Chen, L.Q.; Chen, C.F. Mechanism of (Mg, Al, Ca)-oxide inclusion-induced pitting corrosion in 316L stainless steel exposed to sulfur environments containing chloride ion. *Corros. Sci.* **2013**, *67*, 20–31. [[CrossRef](#)]
16. Muto, I.; Ito, D.; Hara, N. Microelectrochemical investigation on pit initiation at sulfide and oxide inclusions in type 304 stainless steel. *J. Electrochem. Soc.* **2009**, *156*, 55–61. [[CrossRef](#)]
17. Choi, J.Y.; Kim, S.K.; Kang, Y.B.; Lee, H.G. Compositional evolution of oxide inclusions in austenitic stainless steel during continuous casting. *Steel Res. Int.* **2014**, *86*, 284–292. [[CrossRef](#)]
18. Liu, C.S.; Yang, S.F.; Li, J.S.; Ni, H.W.; Zhang, X.L. The influence of FeO on the reaction between Fe–Al–Ca alloy and  $\text{Al}_2\text{O}_3$ – $\text{CaO}$ –FeO oxide during heat treatment at 1473 K. *Metals* **2017**, *7*, 129. [[CrossRef](#)]

19. Neerav, V.; Petrus, P.; Richard, F.; Michael, P.; Minna, L.; Scott, S. Transient inclusion evolution during modification of alumina inclusions by calcium in liquid steel: Part I. Background, experimental techniques and analysis methods. *Metall. Mater. Trans. B* **2011**, *42*, 711–719.
20. Minna, L.; Lauri, H. Transformation of alumina inclusions by calcium treatment. *Metall. Mater. Trans. B* **2010**, *41*, 359–366.
21. Yang, S.F.; Li, J.S.; Wang, Z.F.; Li, J.; Lin, L. Modification of MgO·Al<sub>2</sub>O<sub>3</sub> spinel inclusions in Al-killed steel by Ca-treatment. *Int. J. Min. Met. Mater.* **2011**, *18*, 18–23. [[CrossRef](#)]
22. Eklund, G. Initiation of pitting at sulfide inclusions in stainless steel. *J. Electrochem. Soc.* **1974**, *121*, 467–473. [[CrossRef](#)]
23. JScully, R.; Budiansky, N.D.; Tiwary, Y.; Mikhailov, A.S.; Hudson, J.L. An alternate explanation for the abrupt current increase at the pitting potential. *Corros. Sci.* **2008**, *50*, 316–324. [[CrossRef](#)]
24. Ryan, M.P.; Williams, D.E.; Chater, R.J.; Hutton, B.M.; McPhail, D.S. Why stainless steel corrodes. *Nature* **2002**, *415*, 770–774. [[CrossRef](#)] [[PubMed](#)]
25. Tang, Y.M.; Zuo, Y.; Zhao, H. The current fluctuations and accumulated pitting damage of mild steel in NaNO<sub>2</sub>-NaCl solution. *Appl. Surf. Sci.* **2005**, *243*, 82–88. [[CrossRef](#)]
26. Xu, C.C.; Zhang, X.B.; Li, Z.Q.; Liu, Y.P. Effect of cathodic polarization on chemical and electrochemical states inside occluded cells of localized corrosion of A3 steel. *Corros. Sci. Prot. Technol.* **2000**, *12*, 260–263.



© 2017 by the authors. Licensee MDPI, Basel, Switzerland. This article is an open access article distributed under the terms and conditions of the Creative Commons Attribution (CC BY) license (<http://creativecommons.org/licenses/by/4.0/>).